Broadside interferometric and reverse-time imaging of the San Andreas Fault at depth

Ivan Vasconcelos[⋆], *Stewart T. Taylor*[†], *Roel Snieder*[⋆], *J. Andres Chavarria*[‡], *Paul Sava*[⋆] *and Peter Malin*[†]
[⋆]*Center for Wave Phenomena, Colorado School of Mines, Golden, CO 80401, USA*
[†]*Earth and Ocean Sciences Division, Duke University, Durham, NC 27708, USA*
[‡] *Paulsson Geophysical Services, Inc., Brea, CA 92821*

Summary
The San Andreas Fault Observatory at Depth provides the most comprehensive set of data on the structure and dynamics of the San Andreas fault. We use two independent experiments recorded by the seismometer arrays of the SAFOD Pilot and Main Holes to resolve the localized structure of the San Andreas fault zone and of an intermediate fault zone at depth. From Pilot Hole recordings of the drilling noise coming from the Main Hole, we reconstruct the waves that propagate between the Pilot Hole sensors and use them to image the fault zone structure. The use of correlated drilling noise leads to a high-resolution image of a major transform fault zone. Another independent image is generated from the detonation of a surface explosive charge recorded at a large 178-sensor array placed in the Main Hole. The images reveal the San Andreas fault as well as an active blind fault zone that could potentially rupture. This is confirmed by two independent methods. The structure and the activity of the imaged faults is of critical importance in understanding the current stress state and activity of the San Andreas fault system.

Introduction
The San Andreas Fault Observatory at Depth (SAFOD) was conceived to closely study and monitor the earthquake dynamics and structure of the San Andreas Fault (SAF) at Parkfield, CA. Characterizing the structure and dynamics of the SAF strike-slip system is crucial for understanding the geodynamics of transform plate boundaries and their associated seismicity. Consisting of a vertical borehole, the Pilot Hole (PH), and of a deviated well that intersects the SAF, the Main Hole (MH), SAFOD is designed to sample and monitor the SAF system from within the subsurface at Parkfield.

Figure 1a is a scaled schematic cartoon that summarizes and connects results from several publications that analyze data from the SAFOD site. Much of the information on the surface geology and on the basement and sedimentary structures at Parkfield comes from geologic mapping (Rymer et al., 2003) and from surface refraction (Catchings et al., 2003) and reflection (Hole et al., 2001; Catchings et al., 2003) seismic data. The lateral delineation of the Salinian granite to the SW of the SAF has also been inferred from magnetotelluric (Unsworth and Bedrosian, 2004) measurements and from joint inversion of gravity and surface seismic data (Figure 1b; Thurber et al., 2004). Recent studies of rock samples from drilling (Solum et al., 2006) and well-logs (Boness and Zoback, 2006) from the MH have shed light on the subsurface geology along the SAFOD MH. It was not until 2006 that the SAFOD MH first intersected the SAF (Figure 1a), and the upcoming coring of the SAF system during the Phase 3 drilling of the MH (summer 2007) promises to bring important information on the internal composition of the SAF.

Previous to the drilling of the SAFOD MH, microseismic events along with surface active-shots recorded at the PH seismometer array were used to make some of the first images of the SAF at depth (Chavarria et al., 2003) which also contributed much to our understanding of the subsurface geology at Parkfield (Figure 1a). As a continuation of the subsurface imaging at Parkfield, we use drilling noise recorded at the PH and an active-shot experiment recorded at the SAFOD MH to obtain high-resolution images of the SAF system between depths of 0 to approximately 1.5 km (from sea level; this corresponds to approximately 0.6 to 2.1 km from the surface).

Imaging the SAF from passive and active seismic data
The SAFOD data we use were acquired in two experiments. The first experiment was carried out in July 2004, when the SAFOD PH receiver array (Figure 1b) was switched on to constantly monitor the drilling noise during the early stages of the drilling of the SAFOD MH. We used the drill-bit noise recordings of the SAFOD PH array to create an image of the SAF. In a second independent experiment, conducted in 2005, a large 178-receiver array was placed in the SAFOD MH (Figure 1b) to record the active shooting of an 80-pound explosive charge placed at the surface near the SAFOD MH. To create an image of the SAF zone from the drill-bit noise records we rely on the concept of seismic interferometry (Curtis et al., 2006). Interferometry recovers the response between any two receivers in an arbitrarily heterogeneous and anisotropic medium as if a source was placed at one of the receiver locations (Lobkis and Weaver, 2001). We briefly highlight the issues of interferometry that are of particular concern to the processing of the SAFOD PH drilling noise records.

Removing the contribution of the source power spectrum is an issue when recovering signals from drill-bit noise because in this case the wave-generation mechanism is constantly active, and the spectrum is heavily dominated by specific vibration modes associated to the drilling process (Poletto and Miranda, 2004). This was also observed in these data. The standard industry practice is to estimate the drill-bit signature by placing accelerometers on the drill-stem (Poletto and Miranda, 2004). This estimate is then used to extract the drill-bit noise signature from the cross-

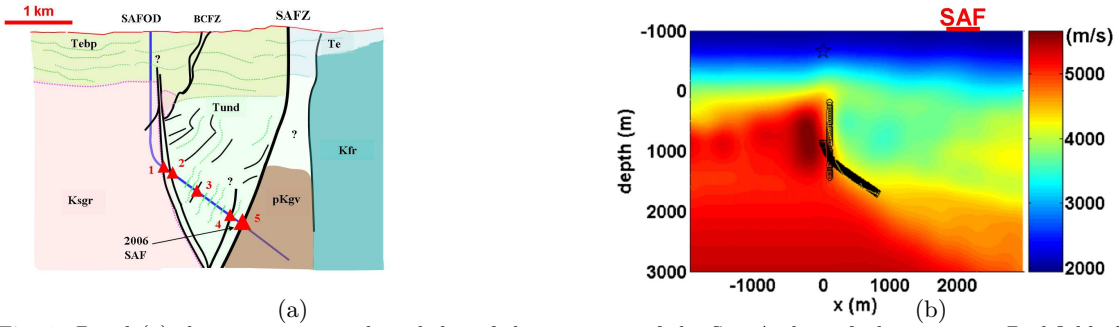

(a) (b)

Fig. 1: Panel (a) shows our current knowledge of the structure of the San Andreas fault system at Parkfield, CA. The main geologic formations are indicated by different colors and by their corresponding acronyms, these are: the Tertiary Ethegoin (Te), Tertiary Ethegoin-Big Pappa (Tebp), Tertiary undifferentiated (Tund), Cretaceous Franciscan rocks (Kfr), Cretaceous Salinian Granite (Ksgr), and the pre-Cretaceous Great Valley (pKgv). The SAFOD main-hole (MH) is indicated by the blue solid line. Black solid lines in (a) represent faults. BCFZ refers to the Buzzard Canyon Fault zone. The areas where the finer-scale structure of the SAF system were unknown are indicated by question marks. The red triangles, numbered 1 through 5, show approximate locations of intersections of the MH with major zones of faulting (Solum et al., 2006). Triangle number 5 represents the point where the MH penetrated the SAF in 2006. Panel (b) shows the large-scale structure of the P-wave velocity field (velocities are colorcoded) that approximately corresponds to the schematic representation in (a). The circles in (b) indicate the location of the sensors of the SAFOD pilot-hole array used here for the recording of drilling noise. The SAFOD MH array, used in the active-shot experiment, is indicated by the triangles. The location of the active shot is depicted by the star. Depth is with respect to sea level, the altitude at SAFOD is of approximately −660 m.

correlations of the recorded data, leaving only the approximate impulse response of the Earth (Poletto and Miranda, 2004). In our case, such accelerometer recordings are not available. As an alternative to interferometry by cross-correlations, we used an interferometry technique based on deconvolutions (Vasconcelos and Snieder, 2007). This technique synthesizes the response between receivers from incoherent excitations as if one of the receivers acted as a pseudo-source, while canceling the effect of the drill-bit source signature without the need for drill-stem accelerometers.

In Figure 2a we show the result from processing approximately 17 hours of drilling noise records into a shot record with a pseudo-source at receiver PH-26. With the pseudo-source centered at 0 s, PH-26 acts as the pseudo-shot responsible for the excitation of waves (Vasconcelos and Snieder, 2007). Figure 2a shows the direct wave that propagates from receiver PH-26 and is recorded at the other receivers. The reflection events highlighted in Figure 2a are caused by faults in the SAF system. The data in Figure 2a represents waves excited by a vertically-oriented force. In addition, we are also able to recover the excitation at receiver PH-26 associated to a Northeast-oriented force (not shown). The SAFOD interferometric image we will discuss here is a product from imaging the pseudo-shots at PH-26 excited by forces oriented both in the vertical and in the Northeast (NE) directions.

The shot gather from the SAFOD MH active-shot experiment (Figure 2b) shows a reflection as a negative-slope event arriving at main-hole receiver MH-98 at approximately 1.0 s (indicated by the top-most arrow). Another weaker negative-slope event that arrives at approximately 1.2 s at receiver MH-98 (lower-most arrow) is associated with a P-wave reflection from the SAF zone. Since the receivers MH-98 to MH-178 are in the deviated, deeper-most portion of the SAFOD MH (see Figure 1b), positive-slope events are mostly associated with right-going waves, whereas negative-slope events are associated with left-going waves. With frequency-wavenumber filtering (Biondi, 2006), we extract only the left-sloping events from Figure 2b. We use only these events to image the SAF zone.

For the imaging of the SAFOD data the velocity model we use is shown in Figure 1b. This model was estimated from surface seismic tomography (Thurber et al., 2004). We do the imaging of the PH and MH data (Figure 2) with two different methodologies. For imaging from the PH data we use the technique of shot-profile migration by wavefield extrapolation (Biondi, 2006). The wavefield extrapolation is done by the split-step fourier phase-shift plus interpolation method. The MH active-shot data in Figure 2b is imaged by *reverse-time migration* (Biondi, 2006).

High-resolution images and the SAF

The images from the SAFOD PH and MH arrays are shown in Figures 3a and b (also in Figures S3a and b). The interferometric image from PH array (Figure 3a) provides a different area of "illumination" of the subsurface than the active-shot image from the MH array (Figure 3b). A numerical model was build for the MH active-shot data to aid us in understanding what is the subsurface area that could be illuminated by the active-shot experiments, as well as what would be the character of image artifacts caused by waves diffracted by the Salinian granite. From the portion of the synthetic image that showed physically meaningful reflectors we chose the area of illumination of the SAFOD MH image in Figure 3b.

We rely on two independent criteria to gain insight into which reflectors in Figure 3 represent real faults

and/or interfaces. The first criterion is based on the consistency of events between different images. Note that all of the available images were generated from independent experiments. Not only were the data in these three experiments different, but also the corresponding images were generated by distinct methodologies. Consequently, reflectors that are consistent in two or more images are likely to be representative of actual subsurface structures. The second criterion for interpreting reflectors in Figure 3 is the correlation between the location of fault zone intersections at the SAFOD main-hole (Solum et al., 2006) and the position of reflectors which are consistent in two or more images. The position of the five main fault zones intersected by the MH are shown schematically in Figure 1a.

In the interferometric image from the PH drilling noise records (Figure 3a) we highlight four distinct reflection events. The events 1 through 3 coincide both in the interferometric and active-shot images (Figures 3a and b, respectively). Reflector 2 (Figure 3) is associated with the SAF, because its lateral position coincides with the lateral position of the surface trace of the SAF (marked by a vertical solid line at 0 km in the background images in Figure 3). In both the PH and MH images, the position of reflector 2 is consistent with the scattering zone associated with the SAF zone from Chavarria et al. (2003). Even though our images of the SAF (reflector 2, Figure 3) do not illuminate the fault all the way to its point of intersection with the SAFOD MH, the change in dip of the SAF in the active-shot image at approximately 1100 m depth is consistent with the intersection of the MH with fault zone 4 (Figure 1a). Since the anomaly that represents the SAF in the image by Chavarria et al. (2003) is caused by direct-wave energy coming from microseismicity within the SAF, the relative positioning between the SAF reflector in the MH active-shot image and the corresponding reflector in the background image suggests that reflector 2 may be due to P-wave energy scattered at the contact of the Franciscan rocks to the NE with the SAF zone to the SW (Solum et al., 2006; Boness and Zoback, 2006).

Although the reflector 1 is consistent between the PH interferometric image and the MH active-shot image, we do not associate it to any known faults. The reason for this is that there is no surface trace of a fault at the location of reflector 1; nor has a major fault zone yet been intersected by the SAFOD MH after the SAF. If reflector 1 is indeed an artifact produced from the imaging procedures applied to both the PH and the MH data, it was not reproduced by the numerical modeling of the SAFOD MH data. Since our modeling was acoustic, reflector 1 could be due to erroneous imaging of recorded P-to-S converted waves.

The fact that reflector 4 can only be seen in the PH interferometric image is not necessarily inconsistent with the MH image because even if the reflector pertained to a physical event, its location makes it mostly invisible for the MH active-shot image (the reflector is located between the shot and most of the receivers in the MH array). The location of reflector 4 suggests a possible correspondence with the SAFOD MH intersection with fault zone number 2 (Figures 1a and S3a). If such a correspondence is true, then reflector 4 is likely to represent the contrast between the Salinian granite and the sediments, which is bordered by fault zone 2 (Figure 1a).

Reflector 3 in Figure 3 is also associated with a fault zone. It is present in both the PH interferometric and in the MH active shot images, and its location coincides with the scattered energy observed by Chavarria et al. (2003) in their P-wave migration images. We associate this reflector with fault intersection number 4 (Figure 1a) in the SAFOD MH array (Solum et al., 2006; Boness and Zoback, 2006). The location of this fault zone at reflector 3 coincides with a well-resolved localized cluster of microseismic events detected both by surface records (Nadeau et al., 2004) and by the PH array (Oye et al., 2004). The imaging of this intermediate fault zone (and its subsequent intersection at the SAFOD PH) is important to the understanding of the structure of the SAF system, especially because there is no trace of this fault system at the surface. Since it is a blind fault (Yeats and Hutfile, 1995; Talebian et al., 2004), determining the activity status of fault 3 is critical in assessing its seismogenic risk. The existence of this feature interpreted from two independent observations provides the basis for a better fault zone understanding and its hazard assessment. Unknown blind faults have been the cause of major earthquakes, such as the 1994 Northridge earthquake (Yeats and Hutfile, 1995) and the 2003 Bam earthquake in Iran (Talebian et al., 2004).

Discussion

Here, we interpret images of the SAF from deconvolution interferometry of drill-bit noise and from active-shot reverse-time migration. Separately, the interpretation of the images is difficult because of the limitations in their respective acquisition geometries. The joint interpretation of the images, however, allows for the identification of the SAF reflector as well as a blind fault zone at Parkfield, CA. In particular, we stress that the use of deconvolution interferometry was key in imaging the SAFOD drill-bit noise because pilot records were not available. The proper manipulation of the SAFOD multicomponent drill-bit records (Vasconcelos and Snieder, 2007b) led to the interferometric image we present here.

The understanding of the structure of the SAF system has gained much from the imaging from the PH drill-bit noise and the MH active-shot experiments conducted at SAFOD. Our current images from these experiments not only provide better resolution in the structural definition of the faults within the SAF, but were also played a decisive role in the characterization of a blind fault zone between the SAFOD PH and the SAF. The high-resolution structural characterization of the SAF system is critical to the understanding of fault-growth and earthquake mechanics at Parkfield. The results we present here prove that imaging from noise can be crucial for illuminating complex fault zones in areas where observations from active experiments are insufficient.

Acknowledgements

This research was financed by the NSF (grant EAS-0609595) and by the sponsors of the Consortium for Seismic Inverse Methods for Complex Structures at the Center for Wave Phenomena.

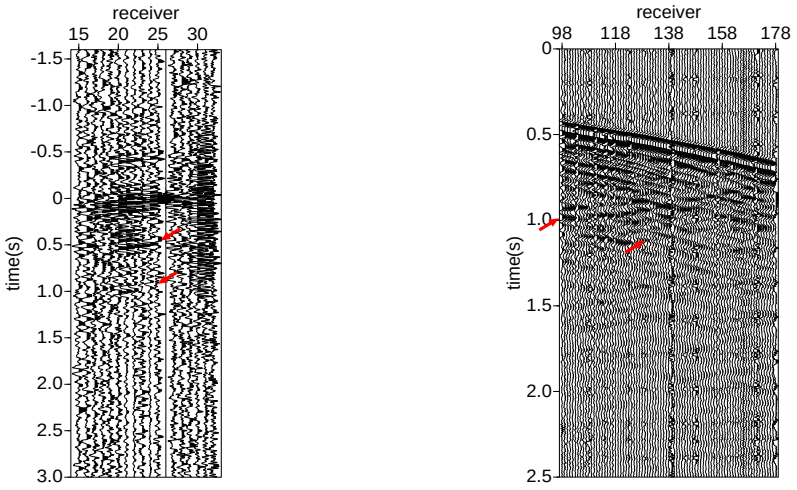

(a) (b)

Fig. 2: (a) Vertical component of the interferometric shot gather for a pseudo-shot position at pilot-hole receiver PH-26. Red arrows indicate reflections of interest. The reflection event that arrives at approximately 1.0 s at receiver PH-24 is interpreted to correspond to a P-wave reflection from the SAF zone. Due to the noise levels, only a subset of the 32 receivers of the PH array is sensitive to the incoming signals from the SAF zone. (b) Data recorded by the vertical component of motion in the SAFOD MH array from the active-shot experiment. The red arrows indicate two left-sloping events that are associated to P-wave reflections from faults within the SAF system.

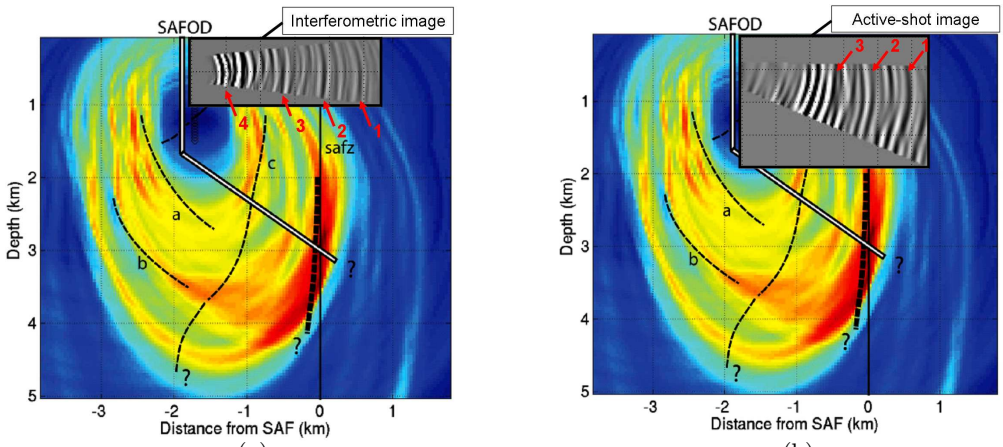

(a) (b)

Fig. 3: Images from the drill-bit noise recordings and from the active-shot experiment (in grey-scale, outlined by black-boxes). These images are overlayed on the result obtained from Chavarria et al. (2003). The overlay in (a) is the interferometric image from the SAFOD PH array, compiled after synthesizing drilling noise records into a pseudo-shot at the location of receiver PH-26. (b) shows an overlay of the image obtained from reverse-time imaging of the active-shot recorded at the SAFOD MH. The arrows mark the most prominent reflectors in the images. The reflectors numbered 1 through 3 coincide in both images. Reflectors 2 and 3, and possibly 4 are associated with fault zones. The SAF zone is visible at reflector 2 in both images. The location of the SAFOD MH in the background color images is schematic, since the MH was drilled after the work by Chavarria et al. (2003) was published. See also Figures S3a and S3b for the full images from the drill-bit noise recordings and active-shot data.

EDITED REFERENCES

Note: This reference list is a copy-edited version of the reference list submitted by the author. Reference lists for the 2007 SEG Technical Program Expanded Abstracts have been copy edited so that references provided with the online metadata for each paper will achieve a high degree of linking to cited sources that appear on the Web.

REFERENCES

Biondi, B., 2006, 3D seismic imaging, investigations in geophysics: SEG.

Boness, N. L., and M. D. Zoback, 2006, A multiscale study of the mechanisms controlling shear velocity anisotropy in the San Andreas Fault observatory at depth: Geophysics, 71, no. 5, F131–F146. .

Catchings, R. D., M. R. Goldman, M. J. Rymer, G. Gandhok, and G. S. Fuis, 2003a, Data report for the main line of the PSINE seismic survey across the San Andreas Fault and the SAFOD site near Parkfield, California: USGS Open-File Report, 03-04:30.

Catchings, R. D., M. J. Rymer, and M. R. Goldman, 2003, Subsurface structure of the San Andreas Fault zone near SAFOD from high-resolution seismic images: Geophysical Research Abstracts, 5, 07861.

Chavarria, J. A., P. Malin, R. D. Catchings, and E. Shalev, 2003, A look inside the San Andreas Fault at Parkfield through vertical seismic profiling: Science, 302, 1746–1748.

Curtis, A., P. Gerstoft, H. Sato, R. Snieder, and K. Wapenaar, 2006, Seismic interferometry - turning noise into signal: The Leading Edge, 25, 1082–1092.

Hole, J. A., R. D. Catchings, K. C. St. Clair, M. J. Rymer, D. A. Okaya, and B. J. Carney, 2001, Steep-dip seismic imaging of the shallow San Andreas Fault near Parkfield: Science, 294, 1513–1515.

Lobkis, O. I., and R. L. Weaver, 2001, On the emergence of the Green's function in the correlations of a diffuse field: Journal of the Acoustical Society of America, 110, 3011–3017.

Nadeau, R. M., A. Michelini, R. A. Uhrhammer, D. Dolenc, and T. V. McEvilly, 2004, Detailed kinematics, structure and recurrence of micro-seismicity in the SAFOD target region: Geophysical Research Letters, 31, L12S08.

Oye, V., J. A. Chavarria, and P. Malin, 2004, Determining SAFOD area microearthquake locations solely with the Pilot Hole seismic array data: Geophysical Research Letters, 31, L12S10.

Poletto, F., and F. Miranda, 2004, Seismic while drilling - fundamentals of drill-bit seismic for exploration: Handbook of Geophysical Exploration, vol. 35.

Rymer, M. J., R. D. Catchings, and M. R. Goldman, 2003, Structure of the San Andreas Fault as revealed by surface geologic mapping and high-resolution seismic profiling near Parkfield, California: Geophysical Research Abstracts, 5, 513.

Snieder, R., K. Wapenaar, and K. Larner, 2006, Spurious multiples in seismic interferometry of primaries: Geophysics, 71, no. 4, SI111–SI124.

Solum, J. G., S. H. Hickman, D. A. Lockner, D. E. Moore, B. A. van der Pluijm, A. M. Schleicher, and J. P. Evans, 2006, Mineralogical characterization of protolith and fault rocks from the SAFOD Main Hole: Geophysical Research Letters, 33, L21314.

Talebian, M., E. J. Fielding, G. J. Funning, M. Ghorashi, J. Jackson, H. Nazari, B. Parsons, K. Priestley, P. A. Rosen, R. Walker, and T. J. Wright, 2004, The 2003 Bam (Iran) earthquake: Rupture of a blind strike-slip fault: Geophysical Research Letters, 31, L1161.

Thurber, C., S. Roecker, H. Zhang, S. Baher, and W. Ellsworth, 2004, Fine-scale structure of the San Andreas Fault zone and location of the SAFOD target earthquakes: Geophysical Research Letters, 31, L12S02.

Unsworth, M., and P. Bedrosian, 2004, Electrical resistivity at the SAFOD site from magnetotelluric exploration: Geophysical Research Letters, 31, L12S05.

Unsworth, M., P. Bedrosian, M. Eisel, G. Ebert, and W. Siripunvaraporn, 2000, Along strike variations in the electrical structure of the San Andreas Fault at Parkfield, CA: Geophysical Research Letters, 27, 3021–3024.

Vasconcelos, I., 2007, Interferometry in perturbed media: Reciprocity theorems, deconvolution interferometry, and imaging of borehole seismic data: Ph.D. thesis, Colorado School of Mines.

Yeats, R. S., and G. J. Hutfile, 1995, The Oak Ridge fault system and the 1994 Northridge earthquake: Nature, 373, 418–420.

no reference in this block